Flexible Grid Connection and Islanding of SPC-based PV Power Converters

Pedro Rodriguez, Fellow IEEE
Abengoa Research
Technical University of Catalunya UPC
Sevilla, Spain
pedro.rodriguez@abengoa.com
prodriguez@ee.upc.edu

Costantino Citro, Ignacio Candela, Member IEEE, Joan Rocabet, , Member IEEE, Alvaro Luna, Member IEEE
Technical University of Catalunya UPC
Barcelona, Spain
candela@ee.upc.edu

Abstract— **Photovoltaic power plants (PV) are equipped with anti-islanding algorithms, embedded in the converters controller, to avoid the island operation. However, the current trends in the development of the future electrical networks evidence that it is technically feasible and economically advantageous to keep feeding islanded systems under these situations, without cutting the power supply to the loads connected to the network. Nevertheless, commercial PV power converters are programmed as grid-feeding converters, and they are unable to work in island mode if there is not an agent forming the grid. In order to overcome this problem the Synchronous Power Controller (SPC) is presented in this paper as a suitable alternative for controlling PV inverters.**

As it will be further discussed this controller permits PV plants to operate seamless in grid connected and island mode, with no need of changing the control structure in any case. Moreover, the participation of SPC based power converters integrating energy storage enables other grid-feeding systems to contribute to the grid operation in island conditions. The results achieved with the SPC will be shown in simulations and also with experiments considering a real PV power plant combining SPC and comercial converters.

Index Terms*— *dc-ac power converters, Photovoltaic systems, Electric variables control, Distributed Power Generation

I. INTRODUCTION

In spite of the increasing penetration of distributed generation systems [1]-[2], the intentional island operation is still not permitted for generation systems which are connected to the main electrical network. Thus, no matter the availability of energy resources, local generation systems are forced to trip when there is an outage in the main grid, with no prejudice of repowering an islanded system after several seconds. However, this operation mode does not prevent the local loads from suffering a total disconnection for some seconds, what in an industrial environment is translated into a complete restart of a production process or a reload of ICT systems [3].

PV based power plants are not an exception among the distributed generation facilities, and they are required to detect the island condition and cease feeding the line with power within a short period of time [4]-[5]. Due to this, the implementation of anti-islanding algorithms is compulsory in all grid-connected PV systems. In this case, the main reason behind this disconnection lays on the fact that a failed disconnection of the power conversion system interfacing a PV plant may result in undesired consequences, such as equipment damages or safety hazard for the grid utility operators.

In order to meet the anti-islanding requirements imposed by the standards, the PV inverter manufacturers include advanced islanding detection algorithms [6]. Among the different solutions, two main categories of islanding detection algorithms are proposed: passive and active methods [7]- [12].

Moreover, at the present time, PV power converters work in grid feeding mode, based on following a current reference. As stated in [13], grid feeding converters cannot work properly if there is no network forming the voltage. Therefore, the anti-islanding standards are not the only issue to be overcame, but it is necessary to find new control methodologies for PV systems in order to enable them to operate either grid-connected or islanded without affecting the operation of the network and the plant itself.

Some studies have been published about the a microgrid operation during disconnection and reconnection transitions in front any outage of the main grid, minimizing disturbances in phase and voltage during transitions, [14]-[15]. The operation of the microgrid in steady state is defined by the good performance of controllers implemented in the different DG connected, as well load sharing functionalities with linear and harmonic loads,[16]. However all these solutions require complex control algorithms dedicated exclusively to solve grid forming situations in case of island condition detection.

In this regard, the SPC, which was presented in [17]-[18] and licensed under the patents [19], [20] and [21], constitutes a good alternative for controlling PV power converters under all kind of conditions.

In this paper the application of the SPC in PV converters and its suitable performance when operating in networks, which can be either seamlessly connected or disconnected from the main grid without affecting the power supply to the loads are analyzed. Moreover, in order to demonstrate the compatibility of the proposed controller, the SPC based converter has been connected in parallel with other commercial PV grid-feeding converters and loads, as it will be shown, through simulations and experiments.

II. THE SYNCHRONOUS POWER CONTROLLER

As it is described in [22]-[25] it is possible to control a grid connected generation system, governed by a power converter, in order to reproduce the same performance and dynamic behavior of a classical synchronous generation system.

However, different solutions based on the implementation of the synchronous machine model in the control algorithm have been proposed. In [23]-[24] the behavior of synchronous generator is mimicked in the control of the converter through the machine swing equations with a virtual impedance. This concept is implemented to synchronize the dc-ac converter before connecting to the grids, however once the system is synchronized with the grid the virtual impedance loop is disconnected and the converter acts as a voltage-controlled inverter. In [25] the machine swing equations with the virtual admittance concept are permanently applied in the control loop to generate the current reference. This current reference is compared with the current measure in the current control loop to generate the duties to be send to the power module. This is advantageous as synchronous generation characteristic has no need of grid synchronization, is able to perform single control loop without considering the state of the grid, provides simplicity in the parallelization of generation units, has an inherent grid-supporting capability and a harmonious operation with the rest of the electrical system.

However, taking advantage of the fact that a power converter is a fully controllable device, it is not only possible to emulate the operation of a synchronous generation system, but even to improve it through on-line modifications of the characteristics parameters of the virtual machine. In this regard the SPC constitutes a new and effective solution to integrate power generators driven by power converters –based on power electronics into the electrical network, gathering the main advantages of synchronous generators operation while overcoming their main drawbacks.

A. *Electrical Control Loop*

The electrical interaction in the connection of a conventional synchronous generator can be described by the following differential equation:

$$v(t) = e(t) - R \cdot i(t) - L \cdot \frac{di(t)}{dt} \qquad (1)$$

where v is the AC voltage at the point of connection, e, is the induced electromotive force, i is the current and, finally, RL represents the output impedance of the generator.

This equation can be implemented in the control layer of a power converter, in order to mimic the electrical performance of the synchronous generator. In such case, the impedance is not physically connected at the output of the converter, but it is virtually implemented in the digital controller of the converter. This approach has been extensively used and its performance has been reported in [26]-[28]. However, the virtual impedance structure presents some issues.

The main one lays on the fact that the virtual impedance concept presents serious control problems when the measured current is affected by harmonics, transients or even noise in the measurements.

As reported in [18], the SPC overcomes this issue by implementing an electrical characteristic based on using a virtual admittance, $Y(s)$. In such a way the power converter is controlled as a current source and there is no derivative terms affecting the controller, as it can be seen in the next expression written in the Laplace domain:

$$i = Y \cdot (e - v) \quad ; \quad Y(s) = \frac{1}{R + sL}. \qquad (2)$$

A simplified layout of the proposed controller is depicted Fig.1, where the power converter is presented as current source. This performance is achieved in a real application including an inner current control loop, as it is shown in the layout depicted in Fig. 2, for a PV power converter case.

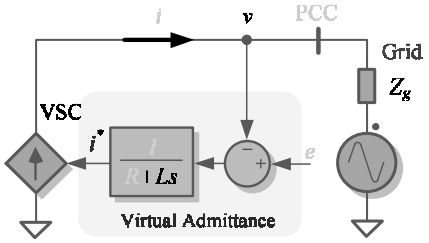

Fig. 1. Electrical control loop based on a virtual admittance.

B. *Electromechanical Control Loop*

In the SPC controller the electrical control loop gets the reference of the internal electromotive force, e, from the output of the electromechanical model as shown in Fig. 2.

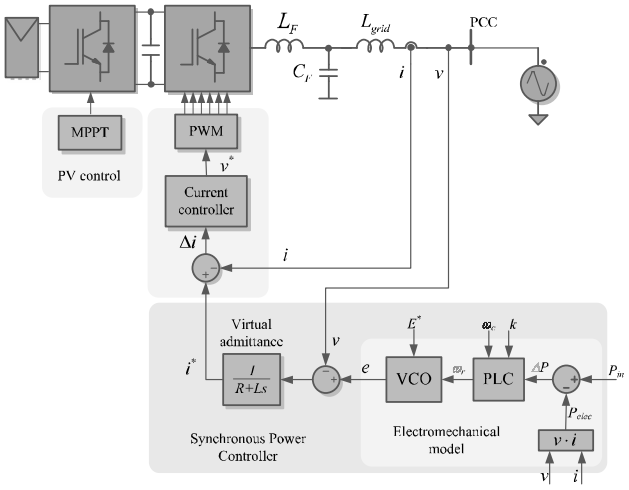

Fig. 2. Electromechanical control loop of the SPC.

The power between the power delivered and absorbed by the converter, ΔP, in a synchronous generator is the one that give rise to the acceleration and deceleration of the mechanical part, changing thus the mechanical speed, ω_r, following the dynamic response of a rotational system. The change in the speed is translated into a variation of the electromotive force in the generator.

Therefore, as stated in [29]-[30], the electromechanical model can implement the same function that is obtained from a real synchronous generator, which involves mainly the inertia of the machine, giving rise to an overall transfer function between the mechanical power (input) and the electrical power (output) in a synchronous generator with very low damping, which is:

$$\frac{P_{elec}}{P_{mec}} = \frac{\omega_n^2}{s^2 + \omega_n^2} = \frac{\frac{P_{Max}}{J \cdot \omega_s}}{s^2 + \frac{P_{Max}}{J \cdot \omega_s}}, \quad (3)$$

where ω_s is synchronous angular speed, J is the inertia of the generator and P_{Max}, which is the theoretical maximum power that an equivalent generator would be able to deliver without hindering the stability.

However, due to the fact that this layer is also fully programmable, an advanced electromechanical characteristic, with controllable damping factor and adjustable inertia, can be programmed. This solution is adopted in the SPC, giving rise to an overall dynamic of the SPC that responds to the following transfer function:

$$\frac{P_{elec}}{P_{mec}} = \frac{\omega_n^2}{s^2 + 2\xi\omega_n s + \omega_n^2}. \quad (4)$$

where ξ is the damping factor and ω_n is the natural frequency of the SPC. As introduced in [17] and [18], this response can be achieved if a Power Loop Controller block (PLC) is introduced, in this case the following transfer function is proposed:

$$\mathrm{PLC}(s) = k\frac{\omega_c}{s + \omega_c}, \quad (5)$$

where the gain k and the cut-off frequency ω_c of the controller can be calculated as a function of the natural frequency ω_n and the damping factor ξ of the closed-loop function as follows:

$$\omega_c = \frac{\omega_n}{2\xi P_{\max}}, \qquad k = 2\xi\omega_n, \quad (6)$$

giving rise to the following virtual inertia in the SPC controller:

$$J = \frac{P_{max}}{\omega_n^2\,\omega_s} \quad \left[\mathrm{kg\,m^2}\right]. \quad (7)$$

The output mechanical frequency of the virtual synchronous generator, ω_r, and its nominal voltage module E^* is converted in $\alpha\beta$ or $dq0$ instantaneous voltage signals, e, in the Voltage Controlled Oscillator (VCO), which performs just a Clarke or Park transformation depending on the reference frame selected for controlling the grid connected power converter.

III. Control in Grid Connected Conditions

One of the main advantages of the SPC lays on the fact that can be implemented in any existing power converter, provided that its current control loop is fast an accurate in order to track the current reference provided by the SPC. As the SPC, implemented in a customized system, as the design of the current controller, based on a proportional-resonant (PR) controller, will be detailed [31].

Considering that the system under control is the one depicted in Fig. 2. The following simplified block diagram can be used for showing the inner control loop structure.

In the current control scheme shown in Fig. 3 a stationary reference frame is adopted on which to implement the control, and a PR is adopted as the current controller. The modulation and acquisition delay is considered in the current control loop in order to conduct an accurate modeling and tuning. The expression of this delay is not exclusive and is determined by the switching frequency and the implementation strategy of the modulation. The *LCL* filter is the most extended grid connection filter, in this case a *LCL* plus a trap filter for the switching frequency has been selected, giving rise to a 5th order system.

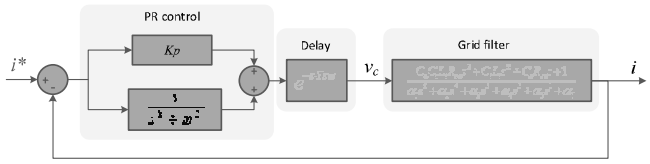

Fig. 3. Structure of the current controller implemented in the inner layer of the SPC controller.

Considering the study case of a 10 kVA grid connected power converter with *LCL*+trap filter, which is the one used in the experimental platform, a *Phm* between [45° 70°] is specified to avoid any undesired oscillations or overshoot during the transient and steady state. Likewise, the *Gm* is selected to be above 10 dB. The final parameters selected for the experimental setup are shown in Table I.

IV. Simulation Results

The structure of the simulation model implemented in this paper consists on four grid connected 50 kVA power converters and two loads, as it is presented in 4. Table II shows the most important parameters of the SPC based converters.

A. Steady State Grid Connected Conditions

Initially all the elements involved in the simulation are enabled and grid-connected. The converters of the plants PV_1 and PV_2 are controlled as grid feeding converters, delivering 30 and 20 kW, respectively, at the beginning of the simulation. Both converters are equipped with active anti-islanding algorithm based on sensing the voltage and frequency deviations.

TABLE I
Tuning of the PR Controller in 10kW Setup

Symbol	Quantity	Valuc
K_p	Proportional gain	6.5
K_r	Resonant gain	18.2
P_{hm}	Phase Margin	50º
G_m	Gain Margin	10.3 dB
ω_c	nominal ac frequency	$2.3{\cdot}10^3$ rad
ω_b	Bandwidth	$4.7{\cdot}10^3$ rad
t_{ss}	Settling time	11.7 ms

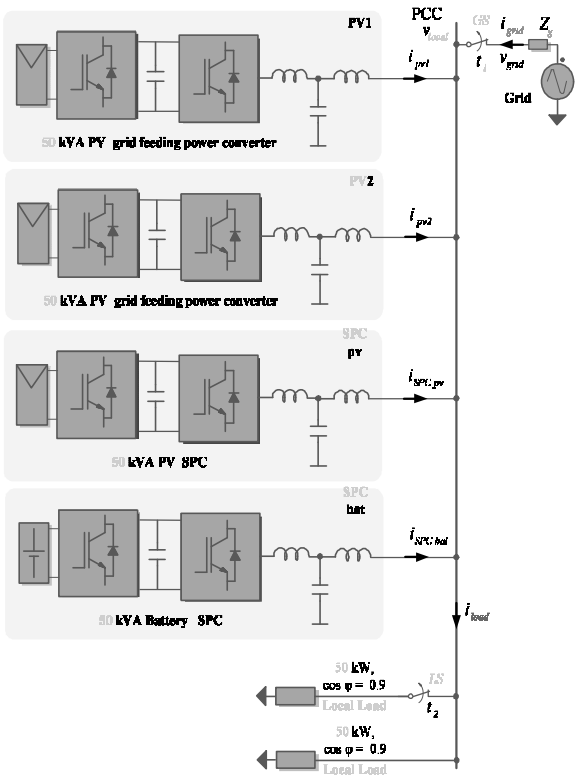

Fig. 4. Simulation study case consisting on: two PV power plants controlled with grid-feeding converters PV_1 and PV_2, a PV plant and a battery controller through a SPC converter, SPC_{PV} and SPC_{BAT} and two 50 kW inductive loads.

TABLE II
SPC CONVERTER TECHNICAL DATA (2 CONVERTERS)

Symbol	Quantity	Value
S_{SPC}	nominal power	50 kVA
V_{DC}	nominal dc voltage	685 V
V_{AC}	nominal ac voltage	400 V
S_{nom}	nominal power	10 kVA
f_{AC}	nominal ac frequency	50 Hz
f_S	switching frequency	10 kHz
L	output filter inductors	0.68 mH
C	output filter capacitors	33 µF
k_P	active power drop ΔP/Δf	100 p.u.
k_Q	reactive power drop ΔQ/ΔV	10 p.u.
H	inertia constant	10 s

B. *Transition to Island Mode Operation*

After operating in the previous grid-connected steady state conditions a fault in the main grid is generated in the simulation at $t = 0.8$ s, which produces a trip of the grid switch (GS), leaving islanded all the PV plants, the ESS and the loads. In Fig. 5 the behavior of the voltage and the currents in the different elements during the transient are depicted.

As it can be seen from these results the voltage in the isolated system, v_{local}, as well as the current required for feeding the load, i_{load}, does not experience any transient that may affect their normal operation between grid connected and island mode, this is due the action of the SPC power converters. This is even more noticeable in the case of the PV converters, as the two conventional plants and the one controlled with SPC remain operative without disconnecting, avoiding the trip that the anti-islanding would generate.

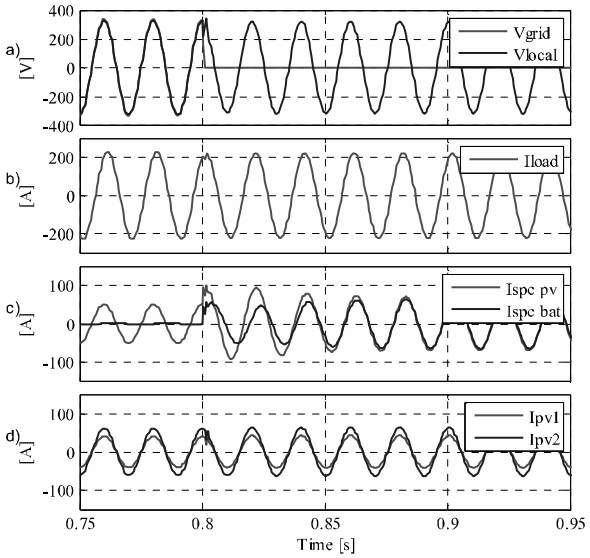

Fig. 5. Performance of the simulated system when there is an outage at t = 0.8 s. (a) Grid voltage and voltage a the PCC; (b) Current absorbed by the load; (c) Current injected by the SPCPV and the SPCBAT; (d) Current delivered by the PV1 and PV2 plants.

This performance evidences the instantaneous and smooth grid forming capability of the SPC, proven by the fact that the anti-islanding algorithms were unable to detect the island.

As indicated previously, all these elements were initially grid connected, so the grid was handling the power balance. However, after the disconnection from the grid there is an unbalance between the power generated and consumed in this test grid. Due to this, the SPC converter belonging to the SPC_{BAT} adapts the power delivery supplying the required active and reactive power for keeping the voltage and the frequency of the system, as it can be noted in Fig. 5 (a) - (b). The change in the power delivery coming from SPC_{BAT} can be understood from the variation of the injected current in Fig. 5 (c).

Moreover, due to the inertia emulation, the SPC_{PV} experiences as well a transient increase of the power delivered to the grid, in order to support the network frequency. This effect is due to the inertia, which extracts the power from the dc bus of the inverter, hence the shape of the currents delivered by the SPC_{PV} go back to their initial value after some milliseconds, as it can be noticed in

Fig. Fig. 5(c).

During the island the reactive power required by the load is shared between the two SPC based converters, which count on the same Q-V droop coefficients, with influence on stationary response, and equivalent output impedance, with influence on transient response. On the contrary the conventional plants, PV_1 and PV_2, remain injecting the power demanded by the MPPT algorithm, and do not take any action for balancing either the reactive power. With a voltage variation of -5 V and

a frequency change of -0.7 rad/s the system reaches finally the equilibrium between generation and load.

C. *Change in the Load when Operating in Island*

Once the system of 4 is working in island mode a change in the value of the load, and thus in the overall energy consumption, has been generated by means of opening the load switch (LS), at t =1.3 s., disconnecting one load of 50 kW with a cos $\Phi = 0.9$.

This change introduces a transient unbalance between power generated and consumed and permits testing the capability of the SPC converters to restore the balance conditions without giving rise to undesired transient that may conduct to the disconnection of the other PV plants, PV_1 and PV_2. The results of this test, at t = 1.3 s, are presented in Fig- 6 and Fig. 7. As it can be observed from the simulation results, Fig. 7 c), the battery-based SPC converter takes care of reestablish the equilibrium point, by means of absorbing the excess of generated power.

During this transient the voltage profile, as well as the currents absorbed by the loads and delivered by the generation systems, do not suffer any undesired transient perturbation, just the change in the average value of the power.

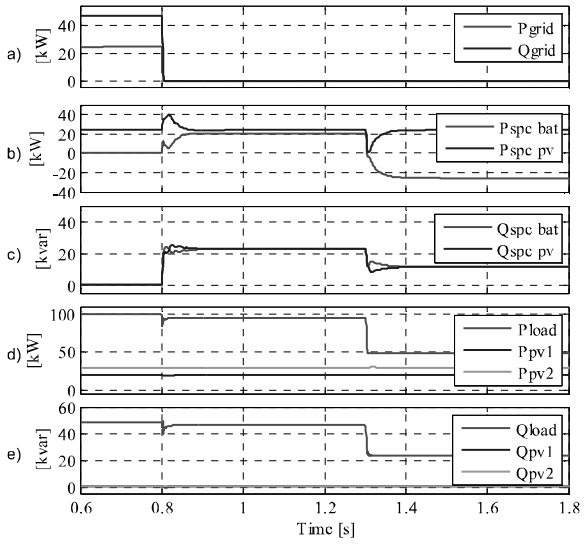

Fig. 6. Power delivery profile considering the network outage at t = 0.8 s and the 50 kW load disconnection at t = 1.3 s. in island mode. (a) Active and reactive power delivered by the grid; (b) Active power delivered by the SPC_{PV} and the SPC_{BAT}; (c) Reactive power delivered by the SPC_{PV} and the SPC_{BAT}; (d) Active power consumed by the load and delivered by PV_1 and the PV_2 ; (e) Reactive power consumed by the load and delivered by PV_1 and the PV_2.

The two SPC converters share the reactive power injection, as it is shown in Fig- 6 (c). As a consequence there is a small variation in the voltage, due to the influence of the grid impedance

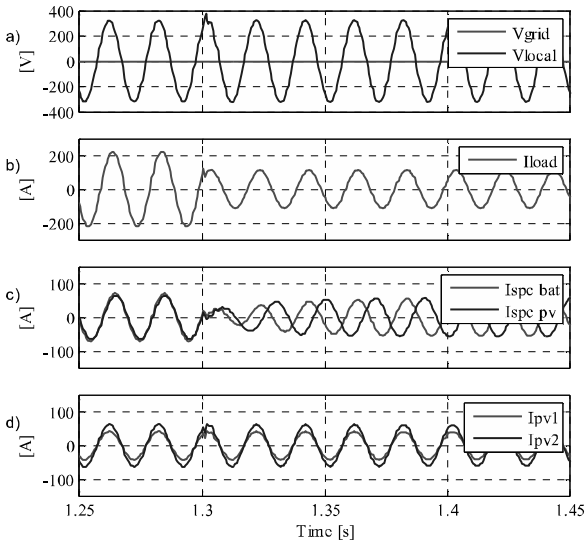

Fig. 7. Performance of the simulated system when there is a change in the load at t = 1.3 s. (a) Grid voltage and voltage a the PCC; (b) Current absorbed by the load; (c) Current injected by the SPC_{PV} and the SPC_{BAT}; (d) Current delivered by the PV_1 and PV_2 plants.

The evolution of the voltage magnitude and frequency is shown in Fig. 8, where it can be stated that they remain within the admissible limits during the entire simulation, from grid connected to island mode including load changes. This window resembles the one that the grid-feeding converters take into account for activating or not the anti-islanding trip, the v-f trajectory is presented in Fig. 9. As in all conditions the deviation in magnitude and frequency is so smalls, thanks to the SPC converter, all the system is able to operate under safe conditions.

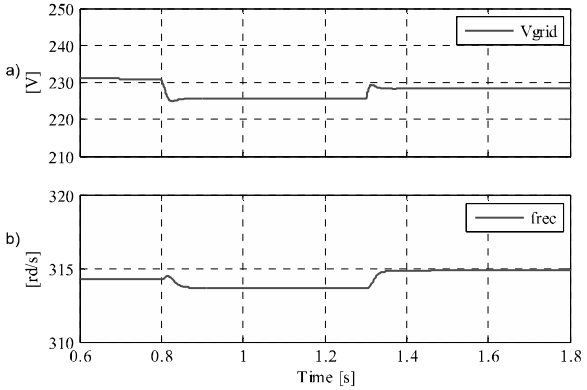

Fig. 8. Performance of the grid variables: (a) Phase to ground RMS value at the PCC; (b) Frequency at the PCC.

V. Experimental Results

The same system used in the simulation has been scaled down and assembled in the lab in order to test the performance of the SPC converter, using two 5 kVA SMA converters linked to a real PV plant and a customized SPC converter.

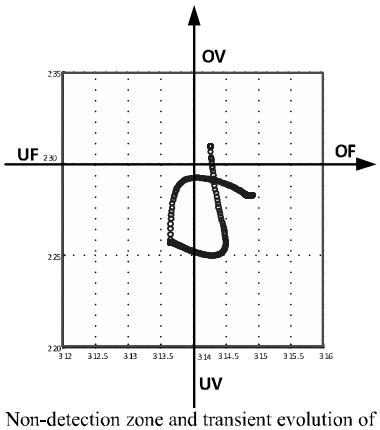

Fig. 9. Non-detection zone and transient evolution of v and f.

A. Study Case

The layout of the experimental platform used in this work is depicted in Fig. 10. As it can be clearly seen, at the point of common coupling (PCC) the main ac system is connected to a local microgrid consisting of four parallelized elements.

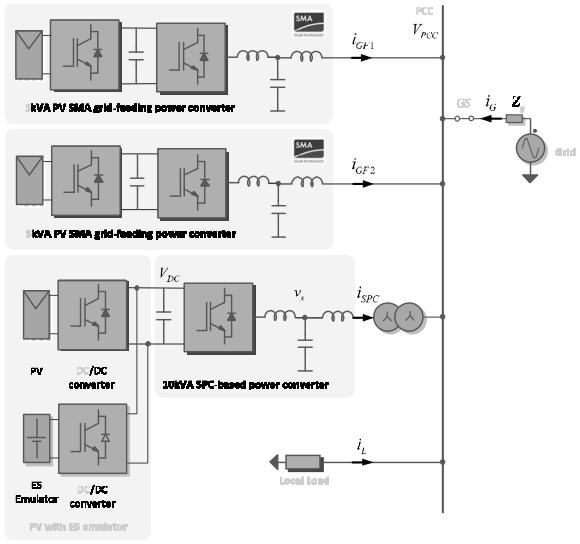

Fig. 10. Structure of the experimental test bench that consist on two 5 kW Tripower converters of SMA connected to PV strings, one 10 kVA converter equipped with SPC controller connected to a PV string, a configurable load and a ES emulator connected to the dc bus of the SPC 10 kVA converter.

The control loops implementation of the SPC-based inverter prototype has been programmed in a TMS28335 floating point DSP of Texas Instruments, and the overall sensed signals have been gathered with an ACE1103 dSpace, which has been used for recording the results of the experiments. All the technical parameters of the system are reported in Tables III and Table IV.

However, as a previous stage in the experimental validation, the SPC implementation has been validated in a HIL600 platform of Typhoon shown in Fig. 11. The SPC controller method is digitally implemented in a DSP of Texas Instruments, which interacts directly with the simulated converter thanks to the connection bays of the HIL600.

TABLE III
SPC PARAMETERS

Symbol	QUANTITY	Value
R_V	virtual resistance	1.6 Ω
L_V	virtual inductance	15.3 mH
H	virtual inertia constant	5
ζ	damping ratio	1

TABLE IV
SPC BASED POWER CONVERTER TECHNICAL DATA

Symbol	Quantity	Value
S_{SPC}	nominal power	10 kVA
V_{DC}	nominal dc voltage	685 V
V_{AC}	nominal ac voltage	400 V
S_{nom}	nominal power	10 kVA
f_{AC}	nominal ac frequency	50 Hz
f_S	switching frequency	10 kHz
C_{BUS}	dc bus capacitance	2.2 mF
L	output filter inductors	3.4 mH
C	output filter capacitors	4.7 μF

Through them the DSP receives the analog measurements from the RTS and provides the digital signals computed by the DSP to the simulated converters, achieving thus the most realistic scenario before the final experimental test.

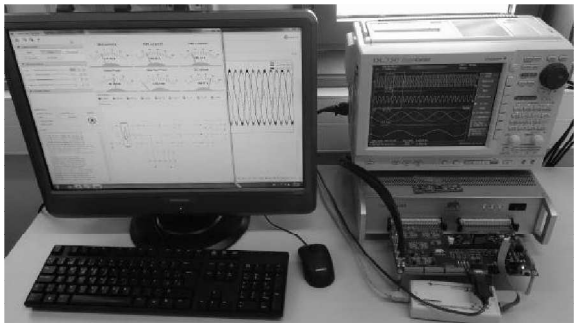

Fig. 11. Simulation platform based on a RTS Typhoon HIL 600 and a TI 28335 Floating Point DSP of TI

This step is of great interest as it reduces greatly the implementation time in the experimental plataform and permits validating the performance on low level controllers when they are embedded in the real digital platform, where the computation time, delays and limitation of memory may affect to the final result.

B. Transition to Island Mode Operation

The possibility of forming an isolated grid is an intrinsic property of a synchronous generator. The experiment presented in this subsection aims indeed at testing the synchronous performances of a SPC-based power converter.

The microgrid illustrated in

Fig. has been set up and the steady state conditions have been reached. With the resistive load absorbing about 10 kW and the PV panels producing about 4 kW, the main ac grid has been suddenly disconnected from the rest of the system.

In a conventional situation the anti-islanding algorithm of the commercial SMA inverters would detect the disconnection of the mains and immediately cease the injection of currents. Nonetheless, the capability of the SPC-based inverter to act as a grid-forming element during and after the mains disconnection makes the anti-islanding system of the SMA inverters not able to detect the occurred transition and continues the PV power production without interruption. The recorded waveforms of the three-phase currents absorbed by the load and the ones generated by the PV panels are shown in in Fig. 12 and Fig. 13 respectively.

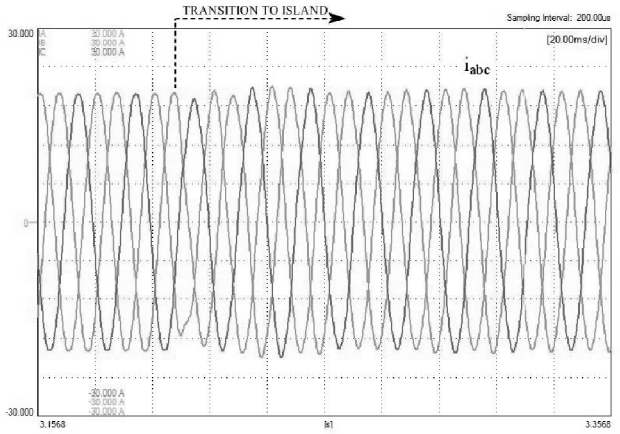

Fig. 12. Three-phase currents (i_L) absorbed by the load (6A/div; 20ms/div).

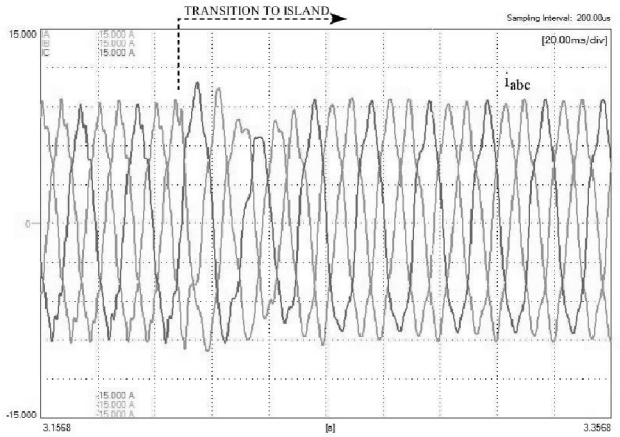

Fig. 13. Three-phase currents ($i_{GF1} + i_{GF2}$) produced by the PV panels (3 A/div; 20 ms/div).

As visible from the figures, a small perturbation in both the load and PV currents is registered as a consequence of the transition to island mode, in part induced by the drop of the grid currents to zero, shown in Fig. 14.

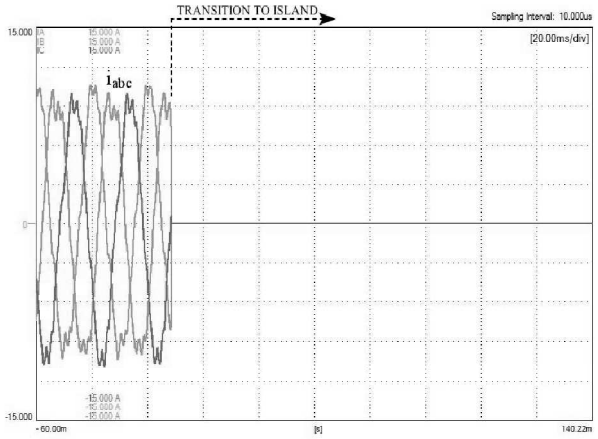

Fig. 14. Three-phase currents (i_G) supplied by the main ac grid (3 A/div; 20 ms/div).

After the mains disconnection, the SPC-based converter automatically intervenes as a grid-forming element. In order to compensate the difference between the power produced by the PV panels and the one demanded by the three-phase resistive load, it automatically increases the amount of injected currents, as visible from Fig. 15. It should be noted that the magnetizing currents absorbed by the isolating transformer give rise to slight distortions in the measurements.

The main objective of the SPC is to keep, as much as possible, stable the three-phase voltage at the PCC, thus allowing the whole microgrid to carry on operating with no interruption.

As visible from Fig. 16, except for the small perturbation registered during the transition to island mode, the quality of three-phase voltages generated by the SPC-based converter is comparable with the one provided by the main ac system prior to the transition.

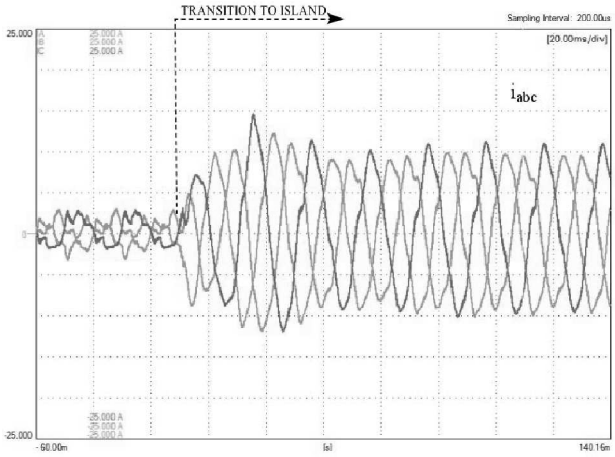

Fig. 15. Three-phase currents (i_{SPC}) provided by the SPC-based converter (5 A/div; 20 ms/div).

The profile of active power generated/absorbed by the different elements connected to the microgrid during the experiment is finally shown in Fig. 17.

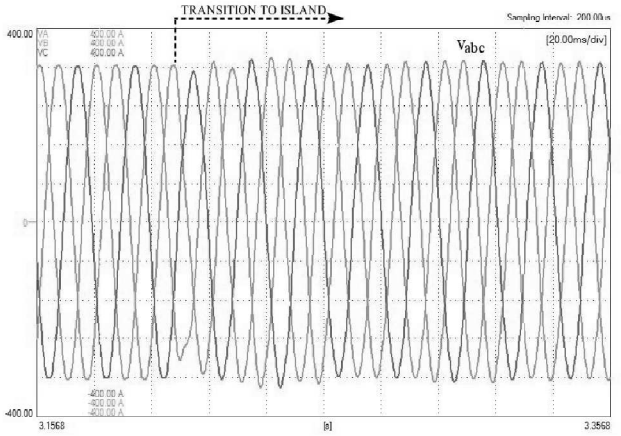

Fig. 16. Three-phase voltages profile at the PCC (80 V/div; 20 ms/div).

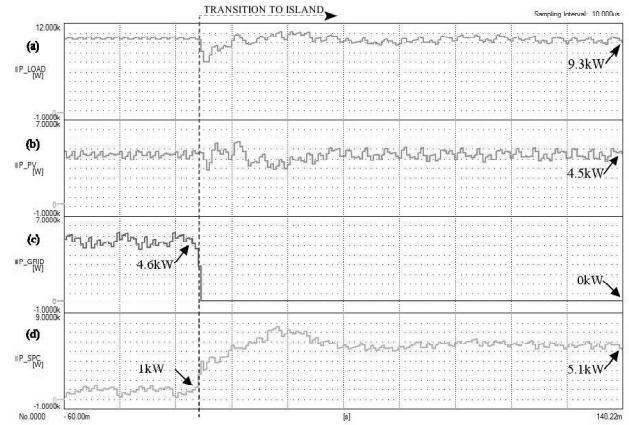

Fig. 17. (a) Active power absorbed by the load; (b) Active power injected by the PV panels; (c) Active power injected by the grid; (d) Active power injected by the SPC-based converter.

The obtained results test the synchronous performances of the SPC-based converter and prove its high capability of acting as a grid forming element during a transition from grid-connected to island mode. The good performance of the system keeps the voltage at the PCC within the limits specified by regulations, thus is not required the intervention of anti-islanding algorithm present in modern commercial PV inverters.

C. Synchronization and Reconnection to the Main ac Grid

The experiment presented in this subsection aims at testing the performances of a SPC-based switching power converter to re-synchronize the microgrid of Fig. 10 with the main ac system and allow a safe and smooth transition from intentional island mode to grid-connected mode. In order to carry out this task, the SPC performs a process of grid-synchronization that brings the microgrid at the same conditions of the main ac grid in terms of voltages (same amplitude, same frequency and same phase). During the whole process of synchronization the anti-islanding system of the SMA inverters must not detect the island condition thus ensuring the continuity of the PV power production.

After operating the microgrid of Fig. 10 in island mode, with the resistive load absorbing about 10 kW and the PV panels producing about 6 kW, the process of synchronization has been manually started. The following Fig. 18 and Fig. 19 show the microgrid voltage and the main ac grid voltage measured in one of the phases at the beginning and at the end of the synchronization.

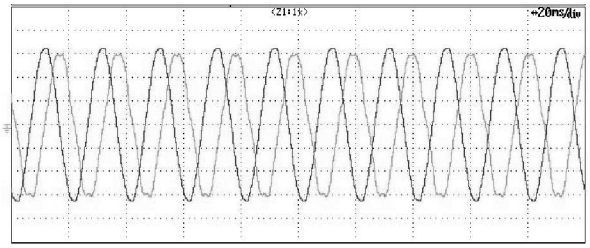

Fig. 18. Microgrid voltage and main ac grid voltage in one of the phases at the beginning of the process of synchronization (100 V/div; 4 s/div).

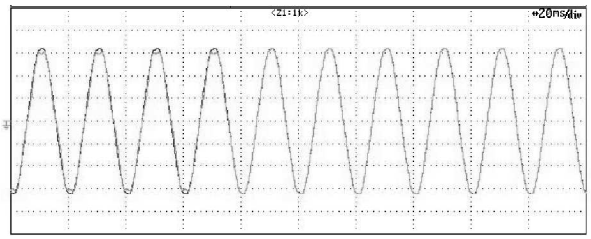

Fig. 19. Microgrid voltage and main ac grid voltage in one of the phases at the end of the process of synchronization (100 V/div; 4 s/div).

Once achieved the synchronization, the external GS of Fig. 10 has been closed, so achieving the transition from island to grid-connected mode. Immediately after the reconnection, for a short instant, some of the power injected by the SPC-based converter is absorbed by the main ac grid, that offers a quite low impedance to the connected microgrid. Subsequently, after a slow transient determined essentially by the inertia constant fixed for the experiment, the output power of the SPC-based converter reaches its internal setpoint, which was manually fixed prior to the reconnection process at 3.3 kW.

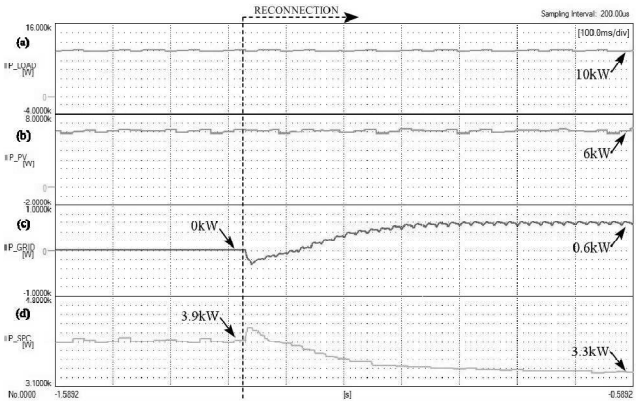

Fig. 40. (a) Active power absorbed by the load; (b) Active power injected by the PV panels; (c) Active power injected by the grid; (d) Active power injected by the SPC-based converter.

During this phase, the behavior of the main ac grid changes: while at the beginning it absorbs some of the power injected by the SPC-based converter, at the end of the transient it injects the necessary amount of power for compensating the difference between the one produced by the SPC-based

converter and the one demanded by the load.

The profile of active power generated/absorbed by the different elements involved during the experiment is finally shown in the following Fig. 20. The obtained results prove the capability of the SPC-based converter to act as a grid forming element and perform a perfect process of synchronization allowing a safe transition of the microgrid from intentional island to grid-connected mode.

VI. Conclusions

In this paper the advantages that the SPC controller introduces in the control of grid connected power converter, its capability to create an isolated network, as well as in the performance of other elements connected to the network, have been demonstrated.

As it has been shown, the implementation of the SPC is simple and it can be integrated in conventional power converter, keeping their inner controller and just adding the additional electrical and electromechanical characteristics.

The advantages of the proposed solution have been particularized for PV applications. In the simulation and experiments performed in this work it has been stated that a SPC based PV power converter is able to operate seamlessly in grid connected and island mode, something that will be required in near future.

As it has been shown, the correct performance of the system is even able to elude the anti-islanding algorithm of the connected commercial PV inverters, something that evidence the soft transitions and lack of undesired transients between grid and islanded operation modes.

Moreover, it is able to prevent the trip of other generation systems, which are programmed to disconnect when the main grid experiences an outage such as grid-feeding power PV power converters, and leave them safely operative feeding the isolated network. In this case it has been also shown how an ESS controlled with SPC is able to regulate the power balance between generation and demand.

The simulation analysis has permitted to validate the good performance when SPC converters are integrated in small scale power plants. Likewise, the 30 kW test-bench have confirmed that no undesired transients appears, even avoiding the anti-islanding protection of a commercial PV converter.

Acknowledgements

This work was partially supported by Spanish Science Ministry under the projects ENE2013-48428-C2-2-R and ENE2014-60228-R. Any opinions, findings and conclusions or recommendations expressed in this material are those of the authors and do not necessarily reflect those of the host institutions or funders.

References

[1] T. Mai, M.M. Hand, S.F. Baldwin, R.H. Wiser, G.L. Brinkman, P. Denholm, D.J. Arent, G. Porro, D. Sandor, D.J. Hostick, M. Milligan, E.A. DeMeo, M. Bazilian, , "Renewable Electricity Futures for the United States," *IEEE Transactions on Sustainable Energy*, vol. 5, no. 2, pp. 372-378, Apr. 2014.

[2] European Commission. (2013, Mar.). "Renewable Energy Progress and Biofuels Sustainability," [Online]. Avaible: http://ec.europa.eu/energy/renewables/reports/doc/2013_renewable_energy_progress.pdf.

[3] K. H. LaCommare and J. H. Eto, Environmental Energy Technologies Division (2004, Sept.). "Understanding the Cost of Power Interruptions to U.S. Electricity Consumers," University of California Berkeley. California. [Online]. Avaible: http://certs.lbl.gov/pdf/55718.pdf.

[4] B.-I. Craciun, T. Kerekes, D. Sera, R. Teodorescu, "Overview of recent Grid Codes for PV power integration," in *Optimization of Electrical and Electronic Equipment (OPTIM)*, 2012, pp. 959-965.

[5] Tedde, M.; Smedley, K., "Anti-Islanding for Three-Phase One-Cycle Control Grid Tied Inverter," IEEE Transactions on Power Electronics, vol.29, no.7, pp.3330-3345, July 2014.

[6] Z. Ye, M. Dame, B. Kroposki. (2005, Jan.). "Grid-Connected Inverter Anti-Islanding Test Results for General Electric Inverter-Based Interconnection Technology," National Renewable Energy Laboratory. [Online] Avaible: http://www.nrel.gov/docs/fy05osti/37200.pdf.

[7] D. Velasco, C.L. Trujillo, G. Garcerá, E. Figueres, "Review of anti-islanding techniques in distributed generators," *Renewable and Sustainable Energy Reviews,* vol. 14, no. 6, pp. 1608-1614, Aug. 2010.

[8] F. De Mango, M. Liserre, A.D. Aquila, A. Pigazo, "Overview of Anti-Islanding Algorithms for PV Systems. Part I: Passive Methods," in *Proc. 12th Power Electronics and Motion Control Conference EPE-PEMC,* 2006, pp. 1878-1883.

[9] S.-H Lee, J.-W. Park, "New Islanding Detection Method for Inverter-Based Distributed Generation Considering Its Switching Frequency," *IEEE Transactions on Industry Applications*, vol. 46, no. 5, pp. 2089-2098, Sept.-Oct. 2010.

[10] G. Hernandez-Gonzalez, R. Iravani, "Current injection for active islanding detection of electronically-interfaced distributed resources," *IEEE Transactions on Power Delivery*, vol. 21, no. 3, pp. 1698-1705, Jul. 2006.

[11] E.J. Estebanez, V.M. Moreno, A. Pigazo, M. Liserre, A. Dell'Aquila, "Performance Evaluation of Active Islanding-Detection Algorithms in Distributed-Generation Photovoltaic Systems: Two Inverters Case," *IEEE Transactions on Industrial Electronics*, vol. 58, no. 4, pp. 1185-1193, Apr. 2011.

[12] H. Karimi, A. Yazdani, R. Iravani, "Negative-Sequence Current Injection for Fast Islanding Detection of a Distributed Resource Unit," *IEEE Transactions on Power Electronics*, vol.23, no.1, pp.298,307, Jan. 2008.

[13] J. Rocabert, A, Luna, F. Blaabjerg, P. Rodríguez, "Control of Power Converters in AC Microgrids," *IEEE Transactions on Power Electronics,* vol. 27, no. 11, pp. 4734-4749, Nov. 2012.

[14] Mohamed, Y. A -R I; Zeineldin, H.H.; Salama, M.M.A; Seethapathy, R., "Seamless Formation and Robust Control

of Distributed Generation Microgrids via Direct Voltage Control and Optimized Dynamic Power Sharing," IEEE Transactions on Power Electronics, vol.27, no.3, pp.1283-1294, March 2012.

[15] Serban, I; Marinescu, C., "Control Strategy of Three-Phase Battery Energy Storage Systems for Frequency Support in Microgrids and with Uninterrupted Supply of Local Loads," IEEE Transactions on Power Electronics, vol.29, no.9, pp.5010-5020, Sept. 2014

[16] Jinwei He; Yun Wei Li; Guerrero, J.M.; Blaabjerg, F.; Vasquez, J.C., "An Islanding Microgrid Power Sharing Approach Using Enhanced Virtual Impedance Control Scheme," IEEE Transactions on Power Electronics, vol.28, no.11, pp.5272-5282, Nov. 2013.

[17] P. Rodriguez, I. Candela, C. Citro, J. Rocabert, A. Luna, "Control of grid-connected power converters based on a virtual admittance control loop," in *Proc. 15th Power Electronics and Applications (EPE)*, 2013, pp. 1-10.

[18] P. Rodriguez, I. Candela, A. Luna, "Control of PV generation systems using the synchronous power controller," in *Proc. Energy Conversion Congress and Exposition (ECCE),* 2013, pp. 993-998.

[19] P. Rodriguez, J.I. Candela, J. Rocabert, R. Teodorescu, "Virtual admittance controller based on static power converters," International Patent WO 2012/117133, Sep. 7, 2012.

[20] P. Rodriguez, J.I. Candela, J. Rocabert, R. Teodorescu, "Controller of the virtual electromechanical characteristics for static power converters," International Patent WO 2012/117133, Sep. 7, 2012.

[21] P. Rodriguez, J.I. Candela, J. Rocabert, R. Teodorescu, "Synchronous power controller of a generation system based on static power converters," International Patent WO 2012/117133, Sep. 7, 2012.

[22] Z. Lidong, L. Harnefors, and H. P. Nee, "Power-Synchronization Control of Grid-Connected Voltage-Source Converters," IEEE Transactions on Power Systems, vol. 25, pp. 809-820, 2010.

[23] Q.-C. Zhong, N. Phi-Long, M. Zhenyu, and S. Wanxing, "Self-Synchronized Synchronverters: Inverters Without a Dedicated Synchronization Unit," IEEE Transactions on Power Electronics, vol. 29, pp. 617-630, 2014.

[24] Q.-C. Zhong and T. Hornik, Control of Power Inverters in Renewable Energy and Smart Grid Integration. Wiley-IEEE Press, 2013.

[25] H.-P. Beck,A. Dowrueng, J. zum Hingst, M.A J M'buy, E--A Wehrmann, "The Clausthal Demonstration Plant for Decentralised Renewable Energy Supply Systems - Clausthal Energy Park -," in *Proc. of. International Conference on Clean Electrical Power ICCEP* , 2007, pp. 41-44.

[26] K. De Brabandere, B, Bolsens, J. Van den Keybus,A. Woyte, J. Driesen, R. Belmans, "A Voltage and Frequency Droop Control Method for Parallel Inverters," *IEEE Transactions on Power Electronics*, , vol. 22, no. 4, pp. 1107-1115, Jul. 2007.

[27] K. De Brabandere, "Voltage and frequency droop control in low voltage grids by distributed generators with inverter front-end"; Ph.D. dissertation, Elec. Eng. Dept. Katholieke Universiteit Leuven, Leuven, België, 2006.

[28] J. Kim, J. Guerrero, P. Rodriguez, R. Teodorescu, K. Nam, "Mode Adaptive Droop Control with Virtual Output Impedances for an Inverter-Based Flexible AC Microgrid," *IEEE Transactions on Power Electronics,* vol. 26, no. 3, pp. 689-701, Mar. 2011.

[29] Q.-C. Zhong, G. Weiss, "Static synchronous generators for distributed generation and renewable energy," in *Proc. of Power Systems Conference and Exposition PSCE*, 2009, pp.1-6.

[30] Q.-C. Zhong, G. Weiss "Synchronverters: Inverters That Mimic Synchronous Generators," *IEEE Transactions on Industrial Electronics,* , vol. 58, no. 4, pp.1259-1267, Apr. 2011.

[31] L. Zhang; L. Harnefors, H.-P Nee, "Power-Synchronization Control of Grid-Connected Voltage-Source Converters," *IEEE Transactions on Power Systems*, , vol. 25, no. 2, pp. 809-820, May 2010.

[32] R. Teodorescu, M. Liserre, and P. Rodriguez, *Grid Converters for Photovoltaic and Wind Power Systems*. 1st ed. Wiley-IEEE press, 2011.